# Modulated Photocurrent Measurements in Double Junction Solar Cells

Nicolás Márquez Peraca and Behrang H. Hamadani

National Institute of Standards and Technology, Gaithersburg, Maryland, 20899, United States

*Abstract* — **Frequency dependent external quantum efficiency (EQE) measurements were performed on double junction solar cells by a custom-designed system consisting of an array of various monochromatic LEDs. LEDs were operated both at constant intensity and pulsed at various frequencies to explore the frequency response of each junction under various conditions. An equivalent circuit model, incorporating the effects of shunt resistances, junction capacitances, optical light coupling and the series resistance was then used to explain the various features and findings obtained from these measurements.**

## I. INTRODUCTION

With significant improvements in design, fabrication, and performance of multijunction solar cells [1,2], it becomes necessary to establish more advanced opto-electronic characterization techniques to explore the characteristics of these solar cells. In recent years, extensive light bias and voltage bias dependent external quantum efficiency (EQE) measurements have been performed to elucidate artifacts and phenomena such as low shunt resistance effects [3,5-8,10,11], reverse breakdown voltage [3,4], light coupling between junctions [9,10,12], etc. in these devices. Most EQE measurements are performed using a differential spectral response system where a monochromatic light source incident upon the cell is chopped at a certain frequency creating an AC signal in the measurement junction of interest, while a DC light bias is applied to the other junctions. Although there has been much work discussing the effects observed under these circumstances, very little work has been dedicated to the frequency response of the AC photocurrent extracted from the current limited junction. One can think of this type of measurement as a frequency-dependent EQE, since the internal junction capacitances and resistances of each junction affect the extracted photocurrent magnitude and phase in the frequency domain.

In this work, we describe the result of our modulated photocurrent measurements in a simple double junction solar cell and show that an equivalent circuit model can be used to describe the unique features observed in both the amplitude and the phase response of the normalized photocurrent or the EQE of these solar cells. In particular, it is demonstrated that EQE shows a significant frequency dependence based on each junction's bias current and capacitive effects.

## II. EXPERIMENTAL DETAILS

A diagram of the experimental setup used for performing the modulated photocurrent measurements is shown in Fig. 1. A function generator is used in conjunction with a custom current amplifier to provide a pulsed AC signal to the LED array, while an LED controller provides the DC input. A solid glass light pipe in the form of a frustum is mounted in front of the LED array, which allows for a uniform illumination spot at the sample location (the exit port of the light pipe) for each LED type used. The cell's output is connected to a high-speed current to voltage pre-amplifier, which in turn is connected to a lock-in amplifier, providing amplitude and relative phase of the signal. This lock-in is synchronized with the function generator, and the whole system is controlled and automated by a computer program. Amplitude and phase dependence of the photocurrent on the frequency of the modulated light can then be found by changing the pulsed LED frequency. To provide stable operation of the LEDs, a water chiller is used to cool down the LED array plate to approximately 15 °C, as shown in Fig. 1.

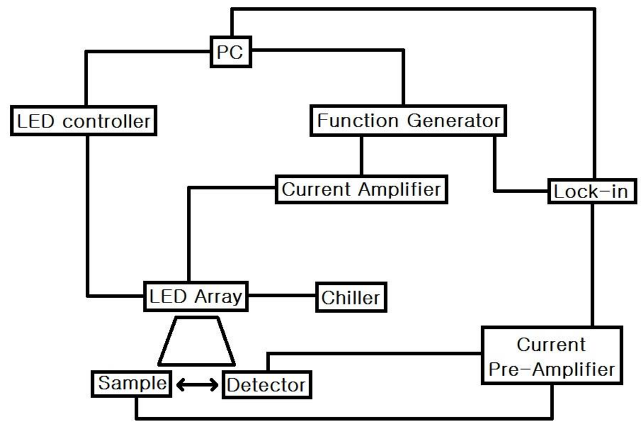


Fig. 1 Experimental setup used for the measurements. Both an AC and DC source are taken as an input of the LED array, which illuminates the sample through a quartz light pipe. A high-speed lock-in amplifier measures the amplitude and relative phase of the signal, and those values are then recorded on a computer.

Fig. 2. shows an actual photo of the optical segment of the setup. The LED array plate can be seen on the left side of the image. It has 12 LEDs of different wavelengths ranging from 460 nm to 928 nm. In this case, both the 460 nm and 623 nm LEDs are turned on, producing a purple color on the sample mounting plate due to the homogenizing of the blue and the red colors passing through the light pipe. The light pipe is in the center, encased in a 3D printed holder.

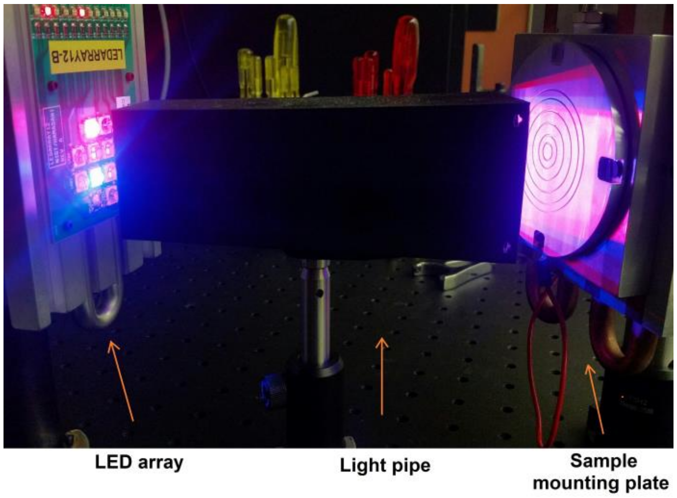


Fig. 2. Photo of the experimental setup. Both 460 nm (blue) and 623 nm (red) LEDs are turned on, producing a purple color at the sample mounting plate.

The solar cell used for this study was a *GaInP/GaAs* cell, with an illuminated active area of 0.2533 $\mathrm{cm}^2$. The top *GaInP* junction is 0.9 $\mu$m thick with a bandgap around 1.84 eV, and the bottom junction is 3.5 $\mu$m thick. The active region of the top and bottom junctions were characterized by performing spectral response measurements on the cell by use of a monochromator-based system (see Fig. 3). Then, 460 nm and 850 nm LEDs were selected for the setup in Fig. 1, the former used as the pulsed light and the latter as bias light. Throughout the measurements the intensity of the pulsed 460 nm LED was kept fixed at 0.5 $W/m^2$.

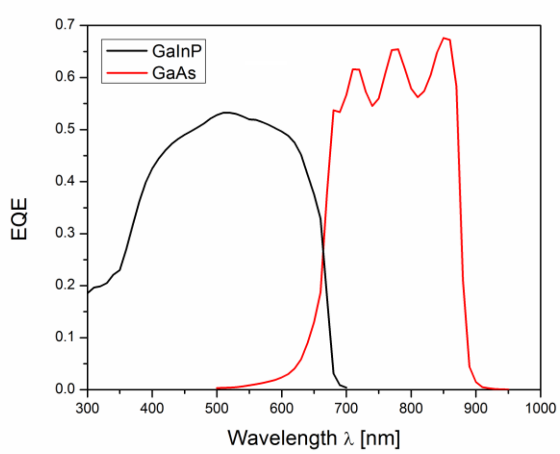


Fig. 3. External quantum efficiency as a function of wavelength for the *GaInP/GaAs* cell, obtained by performing spectral response measurements on the cell by use of a monochromator-based system.

## III. Theoretical Model

An equivalent circuit for the AC light excitation measurements on the double junction solar cell can be seen in Fig. 4. $\tilde{I}_T$ and $\tilde{I}_B$ represent the AC currents generated in each junction, $R_T$ and $R_B$ their dynamic resistances (which might depend on the DC light bias current), and $C_T$ and $C_B$ the depletion region capacitances. The dependent current source $\eta_1 \tilde{I}_r$ models any possible light coupling from the top junction to the bottom. The general solution for the circuit-extracted current, $\tilde{I}_{SC}$ in this model can be found in [9]. In the case where the pulsed light is applied to the top junction while the bottom junction is DC light biased, i.e., similar to EQE measurement conditions for the top junction, this result simplifies to:

$$\frac{\tilde{I}_{SC}}{\tilde{I}_T} = \frac{Z_T}{Z_T + Z_B + R_S} = X(\omega) + jY(\omega)\,, \tag{1}$$

when there is no light coupling from the top junction to the bottom, and:

$$Z_i = \frac{R_i}{1 + j\omega C_i R_i}\,, \tag{2}$$

$$R_B = \frac{nk_BT}{q}\frac{1}{I_B} = \frac{nV_T}{I_B}\,, \tag{3}$$

where $n$ is the diode ideality factor, $k_BT/q$ is the thermal voltage $V_T$ ($\approx$ 25 mV at room temperature), $Z_i$ (for i=T, B) is the complex impedance for the top and bottom junction, $I_B$ is the DC current generated in the bottom junction, and $X(\omega), Y(\omega)$ are the real and imaginary parts of $\tilde{I}_{SC}/\tilde{I}_T$, respectively. It is noted that the ratio $\tilde{I}_{SC}/\tilde{I}_T$ actually represents the internal quantum efficiency (IQE) of this cell because $\tilde{I}_T$, the AC photocurrent generated in the top junction, is proportional to the modulated light intensity, $\tilde{E}_T$. Therefore, the ratio $\tilde{I}_{SC}/\tilde{I}_T \propto \tilde{I}_{SC}/\tilde{E}_T = \tilde{R}_T \propto IQE$, $\tilde{R}_T$ being the internal spectral responsivity of the junction. We have multiplied this value by a fixed constant before comparing the model to the experimental data to include reflectance effects, so that it can represent the EQE at the excitation wavelength probed.

It can be easily seen from (2) that in the low frequency limit where $\omega \to 0$, $Z_i \to R_i$ and so:

$$\frac{\tilde{I}_{SC}}{\tilde{I}_T} \to \frac{R_T}{R_T + R_B + R_S} \approx 1 \tag{4}$$

where the last step follows from the approximation $R_T >> R_B, R_S$ when the top cell is in reverse bias.

On the other hand, in the high frequency limit $\omega \to +\infty$, $Z_i \to 1/j\omega C_i$ and if we consider a negligible series resistance, then we find:

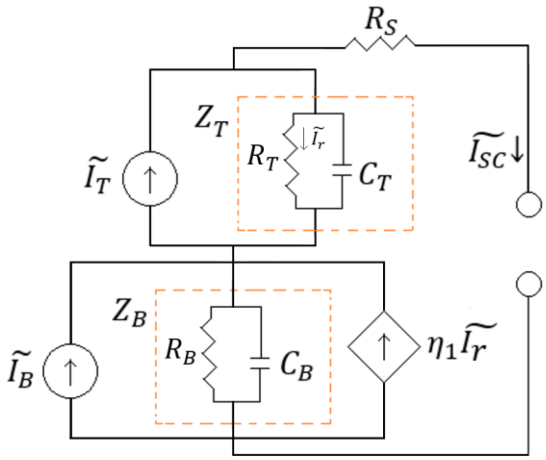


Fig. 4. Equivalent circuit for the AC measurements performed on the double junction cell. The two AC sources represent the currents generated on the junctions, whilst the dependent current source accounts for any possible light coupling.

$$\frac{\tilde{I}_{SC}}{\tilde{I}_T} = \frac{1}{1+\dfrac{Z_B}{Z_T}} \rightarrow \frac{1}{1+\dfrac{C_T}{C_B}} \quad . \tag{5}$$

The ratio $C_T / C_B$ can then be obtained from the EQE($\omega$) plot.

The phase $\theta(\omega) = \mathrm{Arctan}(Y(\omega)/X(\omega))$ presents a resonant behavior and, as it can be seen by taking the quotient of the imaginary and real parts of (1), when there is no series resistance present it goes to zero both in the high and low frequency limits. The value for which this resonant peak happens is found to be:

$$\omega_{\min} = \frac{\sqrt{1+R_B/R_T}}{R_B C_B \sqrt{1+\dfrac{C_T}{C_B}}} \approx \frac{1}{R_B C_B} \propto I_B \ , \tag{6}$$

a result that can be verified by setting the first derivative of $\theta(\omega)$ to zero, and where the last step follows from (3). Furthermore, the real part of $\tilde{I}_{SC}/\tilde{I}_T$ evaluated at this frequency is equal to:

$$\left.\frac{\tilde{I}_{SC}}{\tilde{I}_T}\right|_{\omega=\omega_{\min}} = 2\left[\left(\frac{\tilde{I}_{SC}}{\tilde{I}_T}(\omega\to 0)\right)^{-1} + \left(\frac{\tilde{I}_{SC}}{\tilde{I}_T}(\omega\to +\infty)\right)^{-1}\right]^{-1} \tag{7}$$

On the other hand, a non-zero series resistance causes a drop in the amplitude from the value in (5) to zero, and makes the phase rotate from 0 to -90° in the high frequency limit. Even so, in the region where the condition $\omega_{\min}(I_B) < 1/R_S C_T$ is met the previous analysis continues to be approximately valid.

These features can be seen in Fig. 5, where the left Y-axis represents the magnitude $IQE(\omega) = \sqrt{X(\omega)^2 + Y(\omega)^2}$ and the right Y-axis the phase $\theta(\omega)$, expressed in degrees. Here $R_S$ was kept fixed at $90\,\Omega$ (see next section) while $I_B$ was increased from $0.1\,\mu A$ to $100\,mA$ for exemplification purposes. The curve for $I_B = 100\,mA$ shows the case where $1/R_S C_T < \omega_{\min}$ , and so no resonance is present in the phase plot and the IQE shows a sudden drop to zero at $\omega \sim 1/R_S C_T$ .

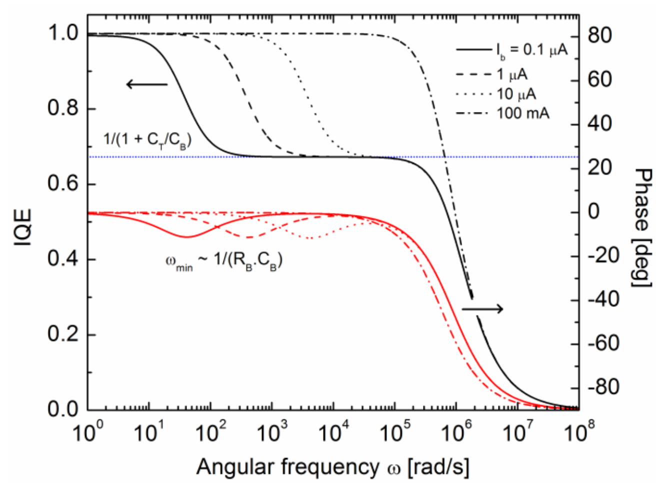


Fig. 5. Predicted internal quantum efficiency as a function of frequency. Here $R_S$ was kept fixed at $90\Omega$ , while $I_B$ was increased from $0.1\mu A$ to $100 mA$ . At the frequency $\omega_{\min}$ , both a resonant behavior for the phase and a sudden drop in the IQE to the value in (5) occur. The high and low frequency limits of (4) and (5) can also be seen in this figure.

## IV. Discussion and Results

Starting from the amplitude and phase data obtained from the lock-in measurements in the experimental setup, both for the solar cell and the reference detector, the external quantum efficiency (EQE) and net phase can be calculated. Fig. 6 shows the results obtained from these measurements (scatter points), as well as the model predictions of (1) (solid lines). The left Y-axis represents the external quantum efficiency and the right Y-axis is the phase, expressed in degrees. Both the model predictions and the measurements were scaled to the EQE value obtained from the monochromator setup at 460 nm, whilst a fixed $\approx 1°$ was subtracted from the phase data to account for the unphysical non-zero phase at low frequencies related to a small phase lag in the instrumentation. The series resistance used in the model was $90\,\Omega$ : $50\,\Omega$ corresponding to the pre-amplifier's input impedance (from the specification data) and $40\,\Omega$ obtained through I-V measurements from the cell itself. Setting 1 to Setting 4 correspond to different DC light bias conditions which, expressed in terms of the LED controller current values, are 1, 2, 5, and 10 mA, respectively.

As Fig. 6 shows, the EQE drop occurs around the same frequency where the phase minimum happens and, as expected from (6), it shifts towards higher frequencies when the DC current generated on the bottom junction increases. This effect suggests that when performing monochromator-based differential spectral response measurements for determining the steady-state EQE of the cell, the chopper's frequency should satisfy the condition $\omega_{meas} < I_B / nV_T C_B$. Otherwise, one risks underestimating the correct magnitude of the EQE for a given junction. In general, it is recommended to perform EQE measurements under the lowest frequencies possible, particularly when light bias conditions are low.

The little discrepancy between the model and the measurements in the high frequency region in Fig. 6 is explained by the fact that our current to voltage pre-amplifier has a strong bandwidth dependence with the source capacitance. For the measured cells having capacitances around 30 nF, the bandwidth drops to approximately 100 kHz to 200 kHz from its maximum value of $\approx$ 100 MHz.

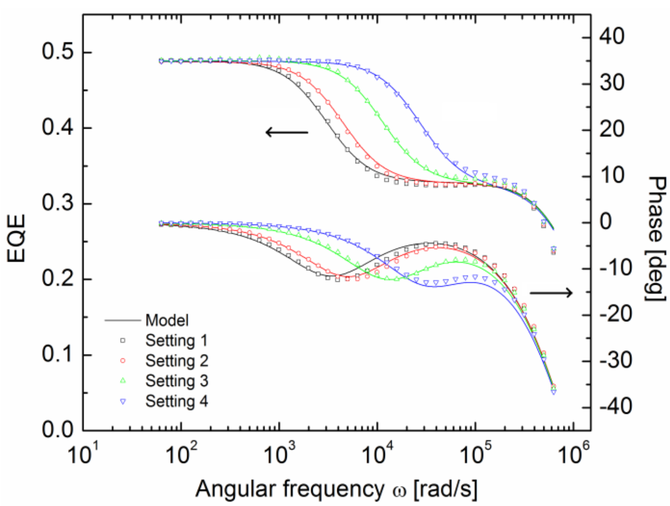


Fig. 6. Results obtained from the measurements superposed to the theoretical model predictions, both being scaled to the EQE reported by the monochromator system. As shown, the optimal measurement frequency depends on the light bias intensity and on the bottom junction capacitance (see text). The values used for the fits were initially estimated from published works, and then adjusted through the model to obtain $C_T = 18.7$ n$F$, $C_B = 38.4$ n$F$, $R_S = 90\ \Omega$, $R_T \approx 10^8\ \Omega$, and $I_B = 8.1\ \mu$A, 11.93 $\mu$A, 30.51 $\mu$A, 74.78 $\mu$A for Settings 1-4, respectively.

## V. Conclusions

Measurements of the amplitude and phase dependence of the external quantum efficiency on frequency for a double junction cell were performed and compared against the predictions of an equivalent circuit model. It was shown that in general the optimal measurement frequency will depend both on the light bias intensity levels and the capacitance of the junction that is in forward bias. Our recommendation is to use a measurement frequency as low as possible, while increasing the light bias. The frequency-dependent photocurrent measurements also allow for the determination of the internal capacitances and resistances of each junction by fitting the described model to a large set of data.

## Acknowledgement


The authors would like to thank Dr. Daniel Friedman of NREL for graciously providing the solar cells used in this study. N. M. P. would like to thank the Solar Energy Laboratory (LES, Uruguay) and the Technological Laboratory of Uruguay (LATU) for their support of the research projects on which he was selected to participate, and to NIST for their hospitality throughout this stay. The authors also gratefully acknowledge the support of the NIST International and Academic Affairs Office.


## References


[1] H. Yoon *et al.*, "Recent advances in high-efficiency III-V multi-junction solar cells for space applications: Ultra triple junction qualification," in *Progress in Photovoltaics: Research and Applications*, 2005, vol. 13, no. 2, pp. 133–139.

[2] M. A. Green, K. Emery, Y. Hishikawa, W. Warta, and E. D. Dunlop, "Solar cell efficiency tables (version 48)," *Prog. Photovoltaics Res. Appl.*, vol. 24, no. 7, pp. 905–913, 2016.

[3] J. P. Babaro, K. G. West, and B. H. Hamadani, "Spectral response measurements of multijunction solar cells with low shunt resistance and breakdown voltages," *Energy Sci. Eng.*, vol. 4, no. 6, pp. 372–382, 2016.

[4] M. Meusel, C. Baur, G. Létay, A. W. Bett, W. Warta, and E. Fernandez, "Spectral Response Measurements of Monolithic GaInP/Ga(In)As/Ge Triple-Junction Solar Cells: Measurement Artifacts and their Explanation," *Prog. Photovoltaics Res. Appl.*, vol. 11, no. 8, pp. 499–514, 2003.

[5] J.-J. Li, S. H. Lim, and Y.-H. Zhang, "A novel method to eliminate the measurement artifacts of external quantum efficiency of multi-junction solar cells caused by the shunt effect," *Proc.SPIE*, vol. 8256, pp. 825616–825623, 2012.

[6] J.-J. Li and Y.-H. Zhang, "Elimination of Artifacts in External Quantum Efficiency Measurements for Multijunction Solar Cells Using a Pulsed Light Bias," *IEEE J. Photovoltaics*, vol. 3, no. 1, pp. 364–369, 2013.

[7] V. Paraskeva, M. Hadjipanayi, M. Norton, M. Pravettoni, and G. E. Georghiou, "Voltage and light bias dependent quantum efficiency measurements of GaInP/GaInAs/Ge triple junction devices," *Sol. Energy Mater. Sol. Cells*, vol. 116, pp. 55–60, 2013.

[8] G. Siefer, C. Baur, and A. W. Bett, "External quantum efficiency measurements of Germanium bottom subcells: Measurement artifacts and correction procedures," in *Conference Record of the IEEE Photovoltaic Specialists Conference*, 2010, pp. 704–707.

[9] M. A. Steiner, S. R. Kurtz, J. F. Geisz, W. E. McMahon, and J. M. Olson, "Using phase effects to understand measurements of the quantum efficiency and related

luminescent coupling in a multijunction solar cell," *IEEE J. Photovoltaics*, vol. 2, no. 4, pp. 424–433, 2012.

[10] J.-J. Li, S. H. Lim, C. R. Allen, D. Ding, and Y.-H. Zhang, "Combined Effects of Shunt and Luminescence Coupling on External Quantum Efficiency Measurements of Multijunction Solar Cells," *IEEE J. Photovoltaics*, vol. 1, no. 2, pp. 225–230, 2011.

[11] M. Pravettoni, R. Galleano, A. Virtuani, H. Müllejans, and E. D. Dunlop, "Spectral response measurement of double-junction thin-film photovoltaic devices: the impact of shunt resistance and bias voltage," *Meas. Sci. Technol.*, vol. 22, no. 4, p. 45902, 2011.

[12] M. A. Steiner *et al.*, "Measuring IV curves and subcell photocurrents in the presence of luminescent coupling," *IEEE J. Photovoltaics*, vol. 3, no. 2, pp. 879–887, 2013.